WFPC-II CCDs

WFPC-II ISR 2-06
M. Clampin, December 1992

SUMMARY

The performance characteristics of the Loral CCDs selected for *WFPC-II* are reviewed to assess their likely impact upon the performance of the instrument. The *WFPC-II* CCDs are thick, frontside illuminated devices with a Lumogen phosphor coating, while *WFPC-I* CCDs are thinned, backside illuminated devices with a coronene phosphor. Based on the results of CCD screening tests at JPL the main conclusions may be summarized as follows:

- **Read noise**: *WFPC-II* CCDs have lower read noise (7 e^-rms) than *WFPC-I* CCDs (13 e^-rms) which improves their faint object and UV imaging capability.
- **Dark noise**: Inverted phase operation yields lower dark noise for *WFPC-II* CCDs. Thus, it is possible to operate at higher temperature (-70°C), which helps in reducing the buildup of contaminants on the CCD windows.
- **Flat field**: *WFPC-II* CCDs have a more uniform pixel to pixel response (<2% pixel to pixel nonuniformity) which will improve the photometric calibration of science images.
- **Deferred charge**: Negligible for *WFPC-II* CCDs so preflash exposures will not be required, reducing overhead time and increasing the faint object imaging capabilities.
- **Dynamic range**: Two CCD gains are available with *WFPC-II*, a 7 e^-/DN channel which saturates at ≈29000 e^- (4096 DN) and a 15 e^-/DN channel which saturates at 61000 e^- (4096 DN).
- **Quantum efficiency**: The Loral devices are thick, frontside-illuminated devices and so have intrinsically lower QE than thinned, backside illuminated devices where there is no attenuation by electrode structures. The peak QE in the optical (400 nm – 1000 nm) is ≈40% (700 nm) while in the UV (110 nm – 400 nm) the QE is ≈10–15%.
- **Residual image**: Tests at JPL show that a residual image resulting from over-illumination by 100×full-well disappears within 15 mins, removing the need for CCD image purging procedures after observations of particularly bright objects.

1 INTRODUCTION

It was originally intended that the *WFPC-II* CCDs would be TI 800×800 CCDs, with Pt bias-gate electrodes to address the problem of quantum efficiency hysteresis (QEH). Subsequently, due to the limited availability of flight quality devices it was decided to design and fabricate a new CCD, based on the TI 800×800 format, at Loral (formerly Ford Aerospace). This report reviews the characteristics of the Loral CCDs and discusses their potential impact on the performance of *WFPC-II*. The main sources for this report are published papers describing the relevant technologies and *WFPC-II* PDR and CDR presentations.

2 *WFPC-II* CCD DESIGN

The *WFPC-II* CCDs are thick, front-side illuminated devices with a format of 800×800, 15×15 μm pixels. They are three-phase devices employing a recent CCD innovation, multi-pinned phase (MPP) (Janesick *et al.* 1989a). MPP allows CCD operation with the total inversion of all phases so that the Si-SiO_2 interface, at the surface of the CCD, can be pinned at the substrate potential, directing signal charge away from the Si-SiO_2 interface states towards the buried n-channel. Figure 1 shows a schematic which illustrates the principle of MPP. Since the frontside Si-SiO_2 interface significantly influences the performance of CCDs (Janesick *et al.* 1989a), MPP operation yields many practical benefits including, reduced dark noise, optimal charge transfer efficiency (CTE), rapid removal of residual images, excellent pixel-to-pixel uniformity and improved improved radiation hardness. MPP technology has been demonstrated and characterized in both Loral (Janesick *et al.* 1989b) and Tektronix devices (Woodgate *et al.* 1989).

3 CCD CHARACTERISTICS

In this section the performance characteristics of the *WFPC-II* CCDs are reviewed and compared to the *WFPC-I* devices. In order to facilitate a rapid comparison a summary of device characteristics is presented in Table 1.

3.1 Read noise

The read noise of the *WFPC-II* CCDs is expected to be $\approx$7 e^-, compared a typical value of 13 e^- for *WFPC-I* CCDs. Note that in practice, the *WFPC-I* CCD read noise is effectively 15–20 e^-, since there are additional contributions resulting from "missing codes" in the analogue to digital convertors (ADC) and the preflash exposure.

3.2 Dark Noise

A reduction in dark noise is one of the benefits of MPP, since inverted phase operation suppresses the dominant source of CCD dark noise production ($Si\text{-}SiO_2$ surface states). The remaining source of dark noise, due to thermal generation in the silicon bulk, is determined by the quality of the silicon used in chip fabrication. The dark noise of *WFPC-II* CCDs is typically <0.01 e^-/pixel/sec at -80 °C, compared to 0.003 e^-/pixel/sec at -88 °C for the *WFPC-I* detectors (*WFPC-I* Handbook 1992).

WFCPC-II should have good UV sensitivity down to 120 nm; the goal is to achieve 1% degradation in UV sensitivity at 147 nm over a period of 30 days. The main impact of the Loral CCDs on the instruments UV capability is their ability to operate at higher temperatures, reducing the rate of condensation of contaminants on the CCD window. The new temperature setpoints for the *WFPC-II* TEC coolers are -90, -83, -76, -70, -50, -40, -30 and -20°C. The approximate dark noise rates for the latter five setpoints are

Temperature (°C)	Dark noise (Counts/s/pixel)
-20	10.0
-30	3.0
-40	1.0
-50	0.3
-70	0.02

It is also possible to perform ambient-temperature imaging which will allow the CCDs to be used for evaluation of the internal instrument alignment during thermal vacuum testing, ground activities prior to launch and the coarse optical alignment phase during SMOV.

3.3 Quantum efficiency

The Loral CCDs are thick, frontside illuminated devices and so their intrinsic QE is lower than thinned, backside-illuminated CCDs due to the absorption of some incident light by the polysilicon electrode structure on the frontside surface of the CCD. The phosphor coating, which converts UV light into the visual range, produces an enhancement of QE at visual wavelengths since it acts as an anti-reflection coating. The UV phosphor selected for the *WFPC-II* CCDs is lumogen, which typically yields gains in QE of 2–2.5 over the *WFPC-I* phosphor coronene. (Trauger 1989). Lumogen also has a long wavelength cutoff (480 nm) which is better matched to the CCD's intrinsic sensitivity. The QE of the four flight *WFPC-II* CCDs is shown in Figure 2 and shows the uniform UV response of 10–15% and a peak optical QE of ≈40%.

3.4 Quantum efficiency hysteresis

The problem of quantum efficiency hysteresis (QEH) due to backside charge accumulation has been reviewed in detail by Griffiths *et al.* (1989) and Janesick and Elliot (1991). The problem is generally associated with thinned, backside illuminated CCDs and is wavelength dependent. QEH should not be present in the Loral CCDs because they are frontside-illuminated and incorporate MPP operation. This is clearly demonstrated by Figure 3 which shows the results of a test for QEH on a *WFPC-II* CCD. The absence of QEH means that the devices do not need to be UV-flooded as for *WFPC-I* and so decontamination procedures can be planned without the constraint of maintaining the UV-flood.

3.5 Charge transfer efficiency

The *WFPC-I* CCDs exhibit low-level non-linearity, known as deferred charge, mainly due to charge traps in the CCD transfer gate, a design fault discussed by Janesick and Elliot (1991) and Griffiths, *et al.* (1989). In practice signal levels (≤ 250 e^-) are effectively smeared over several pixels during transfer. Rectification of the problem requires a preflash exposure (40 e^- pedestal) prior to the majority of science observations, increasing the read noise and adding to the overhead time associated with an exposure.

There are no major deferred charge problems, such as the transfer gate traps, in the *WFPC-II* CCDs. Typically 3–4 low level traps may be present over whole CCD area but they account for a negligible amount of deferred charge ($\approx 200\, e^-$). The absence of any significant deferred charge problem means that preflash exposures will not be required.

3.6 Cosmic rays

For *WFPC-I* a cosmic ray event rate of ~ 2 sec^{-1} CCD^{-1} was measured during SV (Groth and Shaya 1991). This rate should not differ significantly for *WFPC-II* since the detector shielding design is the same as *WFPC-1*. Cosmic ray events will impact scientific imaging with *WFPC-II* in two ways. Firstly, the *WFPC-II* CCDs have an epitaxial thickness of about 10 μm, compared to ≈ 8 μm for the thinned *WFPC-I* device, and a recombination length of 8–10 μm in the substrate (Griffiths priv. comm.). WFPC-II CCDs also have lower read noise and so the overall distribution of cosmic ray event amplitudes will, consequently, differ from that of the *WFPC-I* CCDs since the low amplitude tails will be detected. In practice, this means that in a comparison between *WFPC-I* and *WFPC-II* CCDs the actual number of pixels contaminated by cosmic rays in an image will be higher for the latter, although the event rate is similar. Secondly, the implementation of corrective optics in *WFPC-II* means that stellar images will be undersampled and much more difficult to separate from cosmic rays, as is shown in Figure 4 which compares the predicted *WFPC-II* point spread functions with cosmic ray images from a *WFPC-I* image. Science observations will, consequently, always have to be broken into at least two exposures to ensure that cosmic rays can be identified.

3.7 Dynamic range

The full well capacity of the *WFPC-I* CCDs is ~40000 e^-, but is set in practice by the system gain of 8 e^-/DN and the ADC resolution of 12 bits giving ~30000 e^-. The full-well capacity of the *WFPC-II* CCD, operating with MPP, is large enough to permit a digitized full well of ~70,000 e^-. However, flight qualified ADCs with higher dynamic range (>12 bits) are not available so *WFPC-II* will operate the two available ADC channels with different gain factors. One channel will have a gain of 15 e^-/DN, which significantly undersamples the CCD read noise (7 e^- RMS pixel^{-1}) and gives a digital full well of ~60000 e^-. The other channel will have a gain of 7 e^-/DN, which is comparable to the CCD read noise and gives a digital full well of ~30000 e^-.

The choice of gain factor will be determined by the scientific objective. The 7 e^-/DN channel is best suited to faint object and UV imaging, where the lower CCD read noise will be most effective eg. UV imaging of planets or narrowband imaging of high redshift galaxies. The higher 15 e^-/DN channel gain carries the penalty of effectively higher read noise due to quantization and should be used for programs where a signal level in excess of 30000 e^- is required.

3.8 Residual image

Residuals images in the *WFPC-I* CCDs occur when the full well capacity is exceeded, causing electrons to become trapped at the backside Si-SiO_2 surface interface. Trapped charge is slowly released over a period of time ranging from minutes to several hours, giving rise to residual images. A similar phenomenon, associated with the frontside Si-SiO_2 surface interface, is seen with frontside-illuminated CCDs. Inverted phase operation (MPP) allows holes to recombine with the trapped electrons at the frontside interface and so residual images dissipate very rapidly, on a timescale of minutes. In the case of *WFPC-II* CCDs residual images resulting from a 100×full-well (8×10^6 e^-) exposure disappear very rapidly, so that after ≈1200 seconds no residual image is discernable. Overexposure to charge light levels in excess of 100×full-well has no impact on the image decay time.

A second potential source of residual images, which occur only in frontside-illuminated CCDs, is known as residual bulk image (RBI). Long wavelength photons can penetrate deep enough to produce charge in the substrate. Most of this charge recombines rapidly (due to short carrier lifetimes) but some may diffuse into the epitaxial layer where it can become trapped in epitaxial interface states. Residual images can occur as this charge is slowly released during an exposure. RBI is temperature sensitive since the bulk trapping time constants decrease with increasing temperature. The *WFPC-II* CCDs do exhibit RBI, but at -70°C trapped charge rapidly escapes so that residual images disappear within ≈1000 sec-

onds.

3.9 CCD Flat field

The accuracy of flat fielding is currently one of the major limiting factors in the photometric calibration of scientific observations with *WFPC-I*. The *WFPC-II* CCDs have intrinsically uniform flat field response since they are not thinned, so there are no large scale chip non-uniformities resulting from the thinning process. Furthermore, MPP operation improves pixel-pixel uniformity because charge transfer is driven deep into the buried n-channel away from the influence of Si-SiO_2 interface states. The *WFPC-II* CCD flat fields show an overall pixel-to-pixel response having <2% non-uniformity. There is a low-level ($\approx$3%) fixed pattern resulting from the CCD fabrication. A large amount of dust on the CCD windows currently causes dark spots in the flat fields, but it will be removed prior to integration of the camera assemblies. Figure 5 shows a *WFPC-I* CCD flat field obtained during quantum efficiency measurements at JPL. Despite the fact that there are some artifacts, due to dust and reflections in the optical system, the image illustrates the excellent pixel to pixel uniformity of the Loral devices.

Flat fielding of observations obtained with *WFPC-I* is currently done by using streak flats, obtained by imaging the sunlight earth (see *WFPC-I* SV report). Flat fielding procedures for *WFPC-II* will be different since a dedicated flatfield/calibration module has been incorporated in its design, in addition to the existing method of illuminating the shutter blades currently used for preflash in *WFPC-I*. The flatfield calibration system works by imaging an illuminated diffuser plate onto the WFPC2 exit-pupil (relay secondary), by means of an MgF_2 lens. Two lamps provide optical and FUV illumination providing a flat field which should closely resemble the input beam from the OTA (160 nm-1000 nm). During thermal vacuum testing flat fields will be obtained using the flatfield calibration module and the *WFPC-II* optical stimulus (HST simulator) to generate a database of ratio images which link the internal flats to external flats. The external flats will be verified by comparison against on-orbit streak flats, obtained for a small subset of filters. While streak flats are still required, it is anticipated that they will be obtained during the initial in-flight calibration of the instrument, for verification of the internal flat-fielding procedure, and only used thereafter for periodic calibration checks.

3.10 Radiation damage

In low earth orbit (LEO) the CCDs will be subject to radiation damage from the earth's radiation belts. The WFPC CCDs are shielded from energetic electrons, and about half the incident energetic protons. Long term radiation damage to the CCDs from high energy protons leads to an increase in dark count rate (mainly from the creation of hot pixels), baseline shifts in the CCD amplifiers and long term degradation of CTE. In the case of

WFPC-I a long term dark frame monitoring program has just been established to investigate whether there is an increase in the number of hot pixels. There has not been a significant degradation in the amplifier baselines since launch.

One of the major radiation damage mechanisms is the creation of new Si-SiO_2 interface states which causes increased dark noise. In the MPP-CCD these states immediately recombine with holes reducing the gradual increase in dark noise by factors of ~25 compared to normal three-phase CCDs (Woodgate *et al.* 1989, Janesick *et al.* 1989b).

4.0 CCD Electronics

The CCD camera electronics system are essentially the same design flown on *WFPC-I* with the exception of changes made to implement the different clock pattern for MPP inverted phase operation. Changes in circuit timing have also been made to correct the problem of ADC conversion errors (Lauer 1991).

5 REFERENCES

Groth, E. and Shaya, E., 1991, in *Final Wide Field/Planetary Camera Final Orbital/Science Verification Report*, S., M., Faber, ed.

Griffiths, R. Ewald, S. and Mackenty, J. W. , 1989, in *CCDs in Astronomy*, Proc. A.S.P. Vol. 8, G. Jacoby, ed., 231.

Janesick, J., Elliot, T., Bredthauer, R., Cover, J., Schaefer, R. and Varian, R., 1989a, in *Optical Sensors and Electronic Photography*, SPIE Proc. **1071.**, M. Blouke, D. Pophal, Eds. 115.

Janesick, J., Elliot, T., Blouke, M. and Corrie, B., 1989b, in *Optical Sensors and Electronic Photography*, SPIE Proc. **1071.**, M. Blouke, D. Pophal, Eds. 153.

Janesick, J. and Elliot, T., 1991, in , Proc. A.S.P. Vol.

Lauer, T., E., 1991, in *Final Wide Field/Planetary Camera Final Orbital/Science Verification Report*, S., M., Faber, ed.

Trauger, J. T., 1989, in *CCDs in Astronomy*, Proc. A.S.P. Vol. 8, G. Jacoby, ed., 217.

Woodgate, B. E., 1989, in *CCDs in Astronomy*, Proc. A.S.P. Vol. 8, G. Jacoby, ed., 237.

TABLE 1: Comparison between *WFPC-I* and *WFPC-II* CCDS

PARAMETER	*WFPC-I*	*WFPC-II*
Device	TI	Loral
Architecture	Thinned	Thick
Illumination	Backside	Frontside
Format	800×800	800×800
Pixel size	15 μm^2	15 μm^2
UV Phosphor	Coronene	Lumogen
Dark noise	0.03 e^-/pix/s (-87°)	0.01 e^-/pix/s (-80°)
Read noise	13 e^- RMS	7 e^- RMS
Full well (e^-)	~30000 e^-	~60000 e^-
Gain	8 e^-/DN	(a) 7 e^-/DN (b) 15 e^-/DN
ADC range	12 bits (4096 DN)	12 bits (4096 DN)
QE600 nm	50%	35%
QE250 nm	12%	15%
WFC resolution	0.10 arcsec/pix	0.10 arcsec/pix
PC resolution	0.043 arcsec/pix	0.043 arcsec/pix

Figure 1: A schematic showing the ideal potential profile through a frontside illuminated CCD whose front surface is inverted by Multi-Pinned-Phase (MPP). The CCD structure consists of a polysilicon gate, which forms part of the CCD's electrode structure, a surface layer of oxidized silicon (SiO_2) and the epitaxial layer which comprises p-doped silicon with an N-doped buried-channel for charge transfer. MPP pins the surface potential by populating the Si-SiO_2 interface with holes. The holes passivate the Si-SiO_2 interface states and create an electric field which directs signal charge away from the interface towards the buried n-channel.

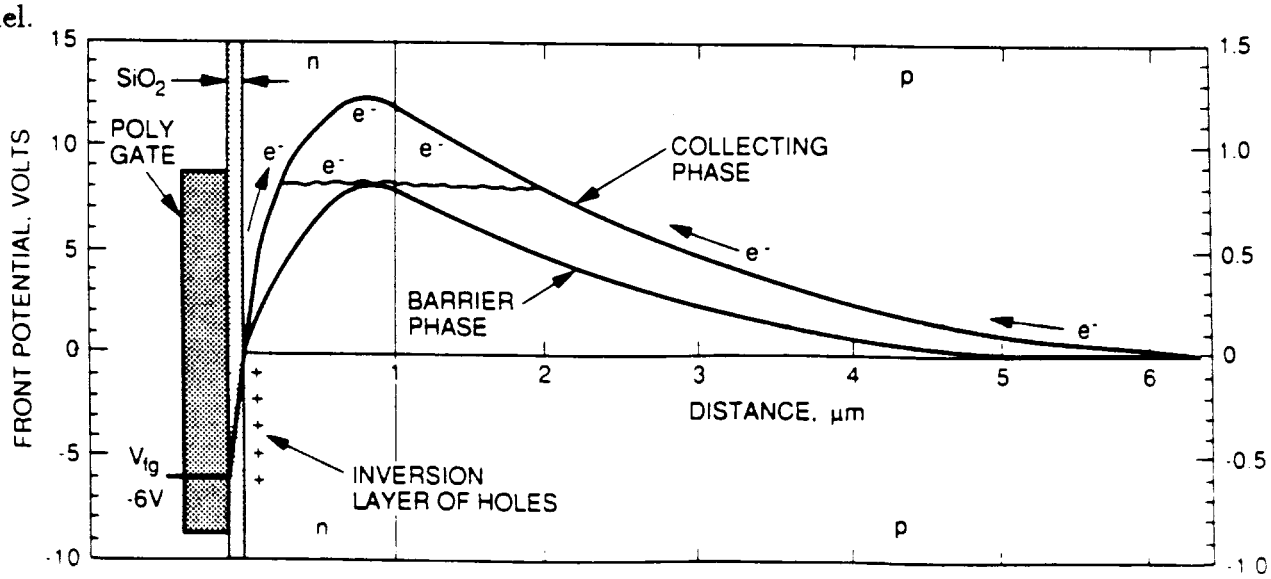

Figure 2: Quantum efficiency curves for the four *WFPC-II* CCDs.

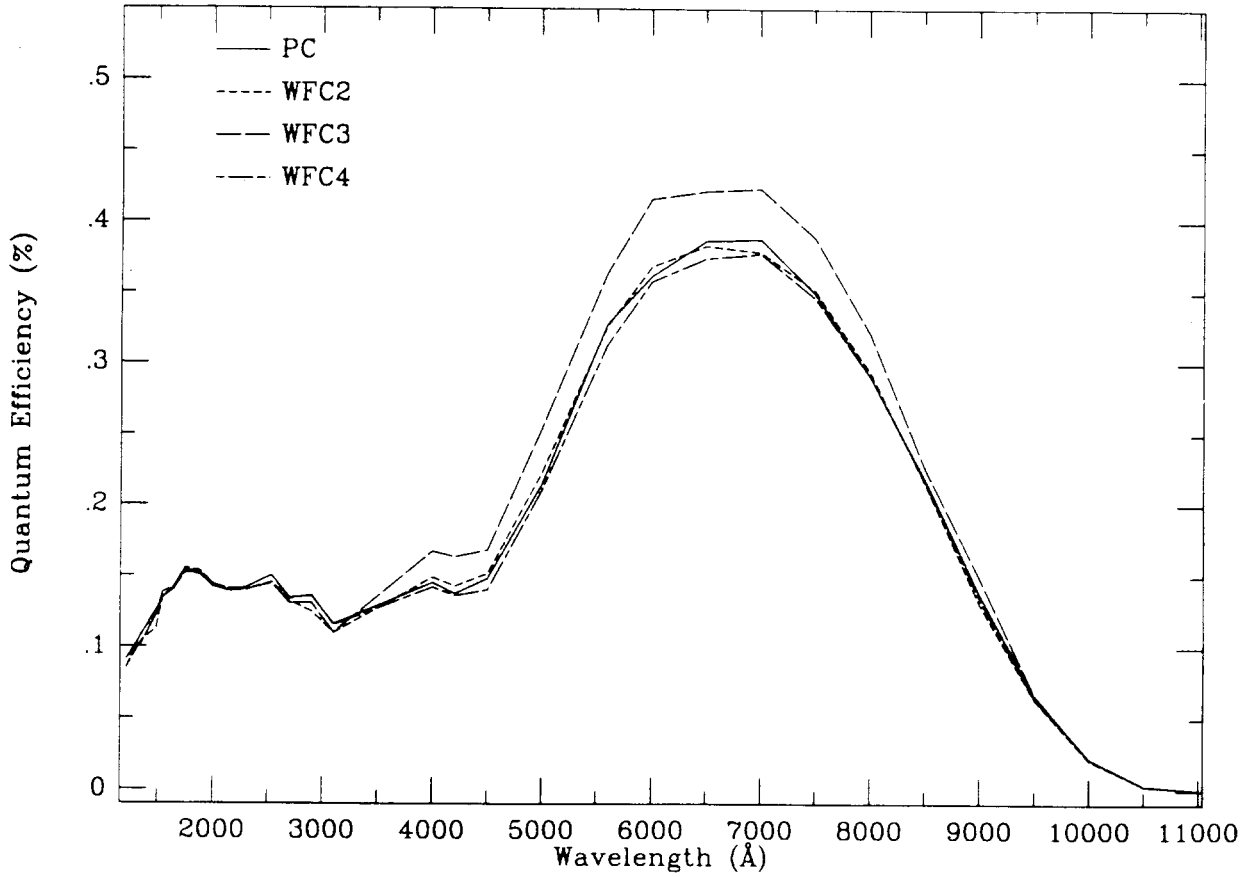

Figure 3: Results of quantum efficiency hysteresis tests for a *WFPC-II* CCD showing the statistics for sub-arrays of CCD pixels for groups of three consective flat field exposures spaced by varying intervals of time (*WFPC-II CDR).*

Figure 4: A simple simulation in which suitably scaled *WF-II* and *PC-II* point spread functions (PSFs), generated using TINYTIM, have been inserted into a section of an internal flat field image obtained *WF-I*. The *WFPC-II* PSFs have been labelled so that they can be compared to the cosmic ray events in the flat field.

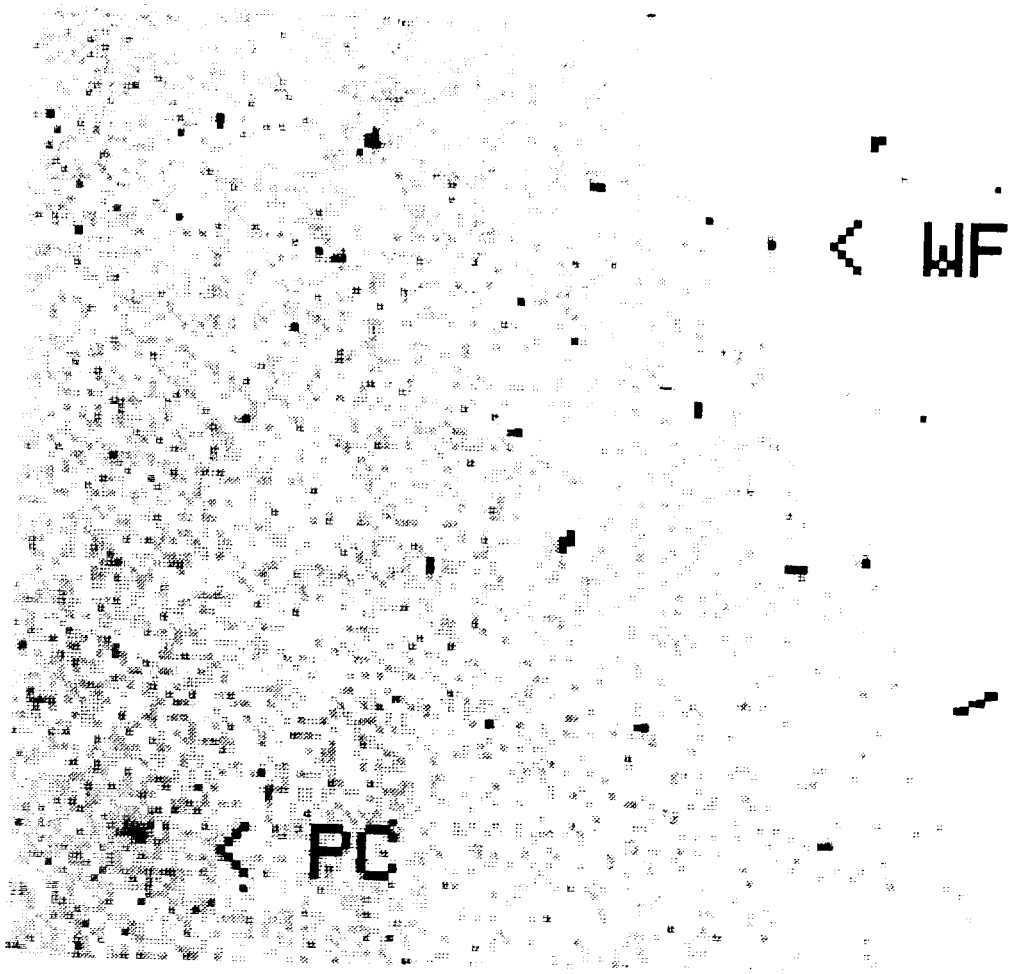
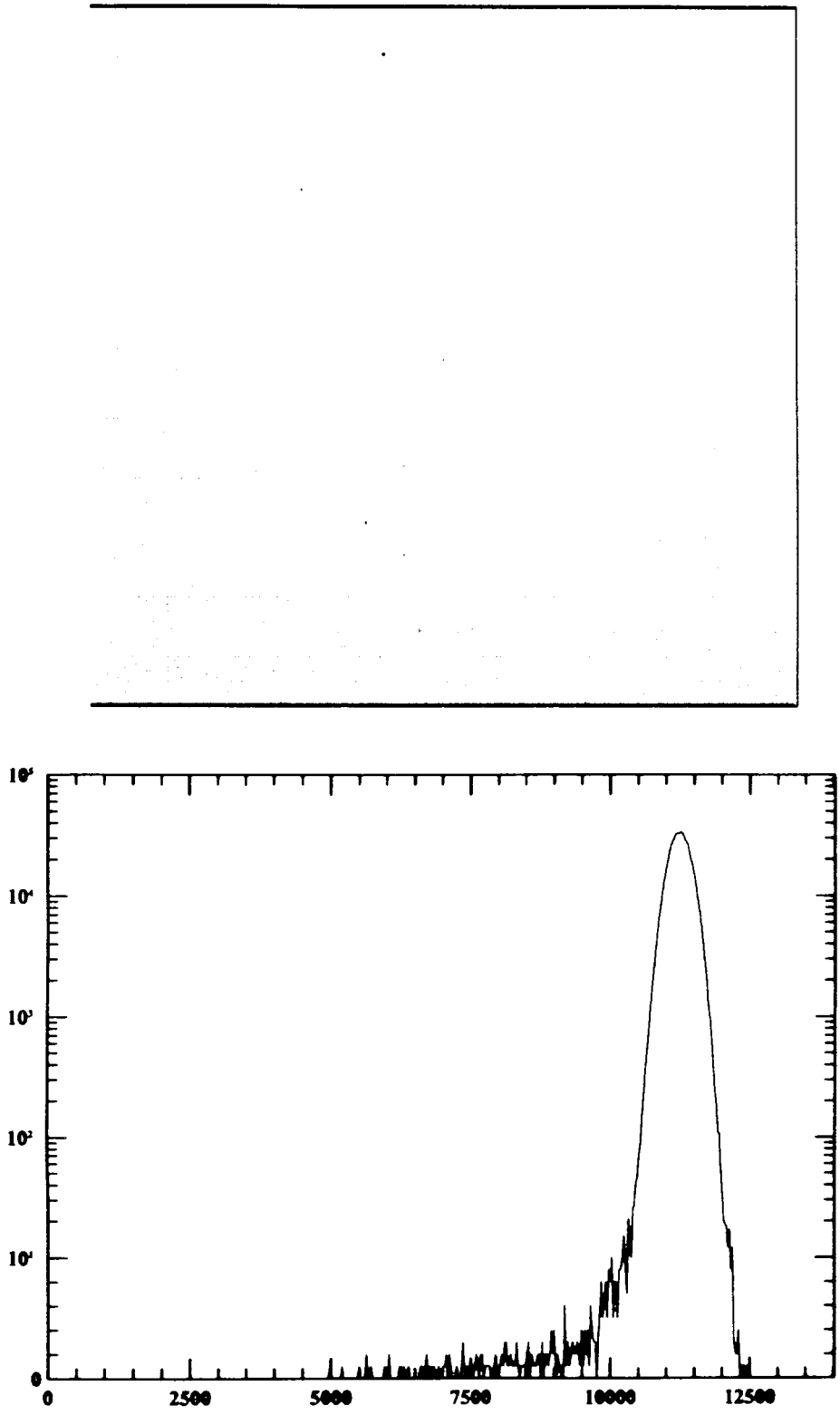
Figure 5: A 400 nm flat field image taken with flight CCD at 400 nm during tests at JPL. A histogram of the image is also shown to demonstrate the uniformity of the flat field.